Journal of CO2 Utilization 57 (2022) 101882

Contents lists available at ScienceDirect

Journal of CO2 Utilization

journal homepage: www.elsevier.com/locate/jcou

Plasma-catalytic CO_2 hydrogenation to ethane in a dielectric barrier discharge reactor

Bryony Ashford [a,b,1], Chee-Kok Poh [b], Kostya (Ken) Ostrikov [c], Luwei Chen [b,d,*], Xin Tu [a,*]

[a] Department of Electrical Engineering and Electronics, University of Liverpool, Liverpool, L69 3GJ, UK
[b] Institute of Chemical and Engineering Sciences, Agency for Science, Technology and Research, 1 Pesek Road, Jurong Island, 627833, Singapore
[c] School of Chemistry and Physics and QUT Centre for Materials Science, Queensland University of Technology (QUT), Brisbane, QLD, 4000, Australia
[d] Department of Materials Science and Engineering, National University of Singapore, 9 Engineering Drive 1, 117576, Singapore

ARTICLE INFO

Keywords:
Plasma catalysis
Non-thermal plasma
CO_2 conversion
CO_2 hydrogenation
Ethane production

ABSTRACT

Anthropogenic greenhouse gas emissions have caused changes to the Earth's climate, resulting in catastrophic weather events that are becoming more frequent and intense. Developing carbon-neutral processes for CO_2 conversion powered by renewable energy is one way of attaining a circular economy, as waste CO_2 is converted to a new carbon-containing product, without also being created as a by-product during the process. Plasma-catalysis is gaining increasing interest for CO_2 conversion and utilisation under mild conditions, particularly CO_2 conversion to green chemicals and fuels using renewable hydrogen, as this electrified process can easily be combined with clean and renewable energy to ensure a carbon-neutral process. Previous studies have mainly focussed on the production of methane from CO_2 and H_2; however, ethane (C_2H_6) is a much more valuable product. In this work, we report a non-thermal plasma-catalytic process for the conversion of CO_2 into C_2H_6 in a dielectric barrier discharge (DBD) reactor. The influence of a variety of alumina-supported metal catalysts (Ru, Cu, Ni and Fe) on the plasma-catalytic CO_2 hydrogenation to C_2H_6 was evaluated. The Ru catalyst attained the highest selectivity towards C_2H_6, at almost 40%. The Ru catalyst also increased the energy efficiency of the process to around 18%, in comparison to the plasma reaction using pure alumina (12%). The Ru catalyst also achieved the highest H_2 conversion at 29%. Plasma-assisted production of C_2H_6 is a new promising process for the utilisation of CO_2 via carbon-neutral electrified gas conversion.

1. Introduction

The 2021 Intergovernmental Panel on Climate Change (IPCC) report unequivocally stated that anthropogenic CO_2 emissions have contributed to climate change and the devastating consequences of this will continue to increase if nothing is done to reduce these emissions. One method of tackling this issue is to develop carbon-neutral processes and energy sources through the utilisation of carbon dioxide. Currently, many industrial processes that use CO_2 as a feedstock rely on high temperatures and pressures to break the strong C═O double bond. These conditions are generated using fossil fuels and increase carbon emissions. Furthermore, production of hydrocarbons via CO_2 hydrogenation reduces our reliance on fossil fuels as hydrocarbons are usually extracted from crude oil. Therefore, developing carbon-neutral and sustainable processes for CO_2 conversion into high-value hydrocarbons has attracted significant interest.

The reaction between CO_2 and H_2 may yield CH_4 or higher hydrocarbons such as gaseous C_2-C_4, along with liquid oxygenates such as methanol, ethanol, acetic acid and dimethyl ether (DME) [1–4]. These valuable products can be used as fuels, or as precursors in the production of other chemicals. In the thermal process, high pressure (1−4 MPa) and temperatures of 200−400 °C are usually required to increase the selectivity towards C_{2+} hydrocarbons [1,2], resulting in the accompanying production of CO_2 emissions. Furthermore, at these conditions, catalyst deactivation due to sintering and carbon deposition remains a challenge in the activation of CO_2 and the growth of carbon chains [2]. Production of higher hydrocarbons (C_{2+}) may require more complex chemistry, but it is favourable in terms of product value. As C_2-C_4 hydrocarbons can be used as fuel, creating a green production process can therefore result in a sustainable energy source.

* Corresponding authors.
E-mail addresses: chen_luwei@ices.a-star.edu.sg (L. Chen), xin.tu@liverpool.ac.uk (X. Tu).
[1] Current address: CSIRO Manufacturing, Lindfield, NSW 2070, Australia.

https://doi.org/10.1016/j.jcou.2022.101882
Received 24 September 2021; Received in revised form 10 December 2021; Accepted 31 December 2021
Available online 22 January 2022

Currently, the electrification of chemical processes has been considered as a promising solution to reduce anthropogenic CO_2 emissions [5] as electricity can be supplied from renewable energy sources, e.g., using photovoltaic or wind power. In the case of the CO_2 hydrogenation process, renewable hydrogen can be generation using water electrolysis. An electrified process that is gaining increasing interest for CO_2 utilisation to C_{2+} hydrocarbons is plasma-catalytic gas conversion. The non-equilibrium nature of plasmas, whereby the bulk gas remains near room temperature whilst the electrons are highly energetic with energies typically in the range of 1−10 eV, dictates that this process has the potential to become a viable method of CO_2 utilisation for the production of hydrocarbons at low temperature and atmospheric pressure [1,2]. Plasma gas conversion is an electric process with very short start-up and shut-down times; thus making it suitable for combining with renewable energy [6], where large fluctuations in energy supply exist, to make a green and sustainable process.

To simultaneously increase the conversion rates and selectivity to different hydrocarbons, and the energy efficiency, a catalyst can be combined with plasmas. The presence of a catalyst in the plasma can affect the discharge properties, increasing the electron energies and local electric field which assists gas breakdown [7–10]. The likelihood of gas phase reactions occurring is therefore increased, leading to higher conversions without the need to raise the discharge power; consequently, the energy efficiency also increases. Furthermore, new reaction pathways emerge at the catalyst surface, which can result in higher CO_2 and H_2 conversion rates and can change the selectivity to different hydrocarbons [5,11]. Non-thermal plasma (NTP) reduces the energy barrier to CO_2 hydrogenation in comparison to conventional thermal processes, thus overcoming kinetic limitations [12] as vibrationally and electronically excited species are produced in the gas phase which can readily interact with the surface of the catalyst and any species adsorbed there [5]. These plasma-catalytic processes are therefore able to selectively produce a variety of hydrocarbons.

Current research on plasma-catalytic CO_2 hydrogenation largely focusses on the production of methane from CO_2 and H_2 [1,5,6,13–20], with only a few studies having been successful in producing higher hydrocarbons and/or liquid fuels [2,3,11,21–23]. However, the mechanisms of selectivity towards higher hydrocarbons and the role of catalyst and support materials remain essentially unclear [12]. The present study fills this knowledge gap by finding effective ways to increase the selectivity towards C_{2+} hydrocarbons using a dielectric barrier discharge (DBD) plasma reactor combined with iron, ruthenium, copper or nickel catalysts.

2. Experimental

2.1. Plasma reactor setup

Fig. 1 shows the structure of the DBD reactor. The outer electrode was formed using aluminium foil, 16 mm in length. This foil was wrapped around a quartz tube (dielectric barrier) with 2 mm wall thickness. The complete experimental setup can be seen in Fig. 2. Throughout these experiments the total flow rate (CO_2+H_2) remained unchanged at 60 mL/min, with a H_2/CO_2 molar ratio of 4:1. 1.6 g of catalyst, supported on Al_2O_3 beads (or pure Al_2O_3 beads) with a diameter of 1 mm, was fully packed into the discharge area. The discharge volume of the empty reactor was 1.8 cm^3 The current was measured by a current monitor (Bergoz CT-E0.5), while the applied voltage was recorded using a high voltage probe (Testec, HVP-15HF). The voltage across an external capacitor was used to measure the charge formed in the DBD plasma. All the electrical signals were sampled using a digital oscilloscope (TDS2014). The discharge power was determined using the Lissajous figure method. The frequency was kept constant at 9 kHz and the discharge power at 16 W. Note that there were also no obvious changes to the electrical signals when packing pure Al_2O_3 or different Al_2O_3 supported catalysts to the DBD reactor. This was because the

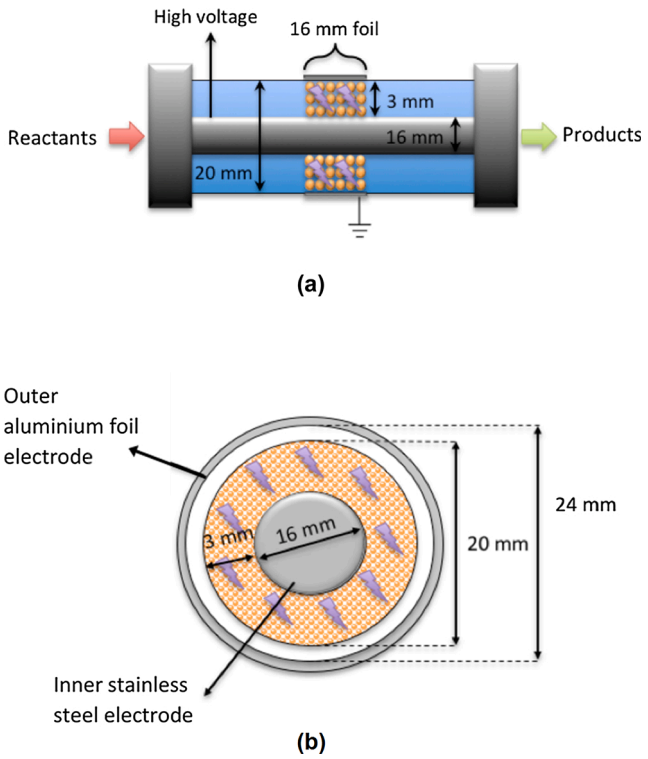

Fig. 1. DBD plasma reactor: a) diagram of packed bed reactor setup; b) cross-sectional diagram of packed bed reactor.

majority of the discharge volume was filled with Al_2O_3, with only 10 wt % of the metal phase, and the properties of the alumina beads remained fairly constant during the experiments. Similar findings were also reported in our previous studies [24]. In addition, the temperature of the catalyst surface was not determined due to difficulties in accurately measuring this value, as a thermocouple cannot be used to measure the plasma temperature in the reactor due to the use of high voltage and the thermocouples' ability to affect the discharge properties. Furthermore, other non-invasive techniques, such as IR temperature monitoring, cannot be used for this experiment as an Al foil was used as the outer electrode and as such the plasma was not visible. However, the adhesive Al foil tape (3 M 425 Al foil tape) used in this experiment can only withstand temperatures of up to ~150 °C. Furthermore, our previous work [25] showed that the temperature in the DBD reactors was typically low (100−200 °C). It has also been shown that packing different catalysts into the discharge zone had limited effect on the plasma temperature compared to the plasma-only system when the discharge power remained constant [25], as is the case in this manuscript. As the Al foil remained stable during the experiment, and given our previous findings, it is reasonable to assume that the temperature in the plasma reactor was below 200 °C and that no significant change to the temperature occurred in the presence of different catalysts.

Gas products were analysed online using an Agilent 3000 MicroGC. This was a 4-channel gas chromatograph; however, only channel 1 (MolSieve 5A) and channel 2 (PLOT Q) were used. The molecular sieve was used to separate H_2, CO and CH_4, whilst the PLOT Q column was used for CO_2, C_2 and C_3 hydrocarbons. This allowed quantitative analysis of the data. The gas was sampled every 4 min over a one-hour period after the plasma was turned on, as well as for 20 min prior to the experiment.

To calculate the CO_2 and H_2 conversions and selectivities to CO and C_xH_y for the CO_2 hydrogenation reaction, the GC was calibrated using a standard gas cylinder containing nitrogen.

The conversions of CO_2 (Eq. 1) and H_2 (Eq. 2) were calculated according to:

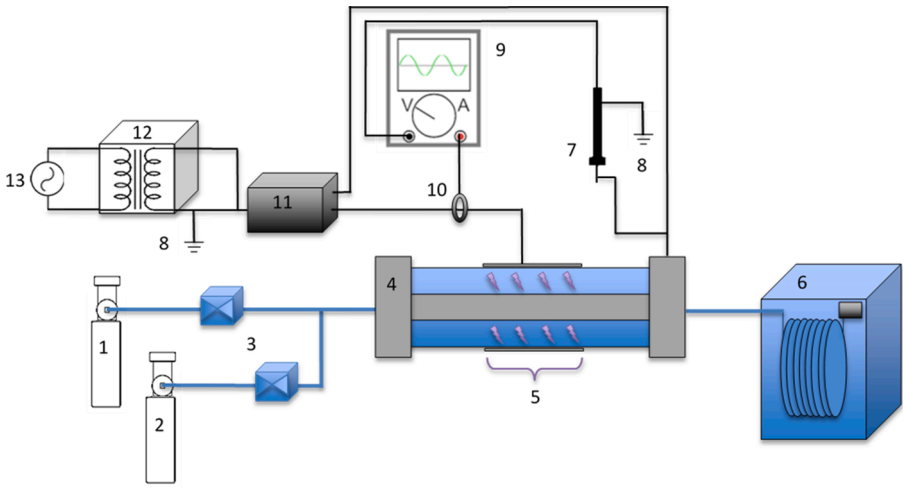

1. CO_2 gas cylinder
2. H_2 gas cylinder
3. Mass flow controllers
4. Dielectric barrier discharge reactor
5. Discharge region
6. Gas chromatograph
7. High voltage probe
8. Earth connection
9. Oscilloscope
10. Current transformer
11. Neon power supply
12. Voltage regulator
13. AC power

Fig. 2. Schematic diagram of the plasma process setup.

$$X_{CO_2}(\%) = \left(\frac{CO_2 \text{ converted (mol/s)}}{CO_{2_{in}}(\text{mol/s})}\right) \times 100\% \quad (1)$$

$$X_{H_2}(\%) = \left(\frac{H_2 \text{ converted (mol/s)}}{H_{2_{in}}(\text{mol/s})}\right) \times 100\% \quad (2)$$

The selectivity to each product was calculated using Eq. 3, where [i] is the concentration of each product.

$$S_i = \left(\frac{[i]}{\sum [CO + CH_4 + C_2H_2 + C_2H_4 + C_2H_6 + C_3H_6 + C_3H_8]}\right) \times 100\% \quad (3)$$

The carbon balance was determined using Eq. 4.

$$B_{carbon}(\%) = \frac{\left(\begin{array}{c} CO_2 \text{ unconverted (mol/s)} \\ +(CO + CH_4 + 2 \times C_2 + 3 \times C_3) \text{ produced (mol/s)} \end{array}\right)}{CO_{2_{in}} \text{ (mol/s)}} \times 100\% \quad (4)$$

The energy efficiency of the process was calculated in terms of energy cost (EC) for each of the two reactants (CO_2 (Eq. 5) and H_2 (Eq. 6); for CH_4 production (Eq. 7); and for C_2H_6 production (Eq. 8).

$$EC_{CO_2}(\text{MJ/mol}) = \frac{\text{Discharge power (kW)}}{1000 \times CO_{2_{in}} \text{ (mol/s)} \times X_{CO_2}(\%)} \quad (5)$$

$$EC_{H_2}(\text{MJ/mol}) = \frac{\text{Discharge power (kW)}}{1000 \times H_{2_{in}} \text{ (mol/s)} \times X_{H_2}(\%)} \quad (6)$$

$$EC_{CH_4}(\text{MJ/mol}) = \frac{\text{Discharge power (kW)}}{1000 \times CH_4 \text{ produced (mol/s)}} \quad (7)$$

$$EC_{C_2H_6}(\text{MJ/mol}) = \frac{\text{Discharge power (kW)}}{1000 \times C_2H_6 \text{ produced (mol/s)}} \quad (8)$$

The energy efficiency of the process was determined using Eq. 9.

$$EE(\%) = \left(\frac{\begin{array}{c}(CO_2\text{converted (mol/s)} \times \Delta H(\text{kJ/mol})) \\ +(H_2\text{converted (mol/s)} \times \Delta H(\text{kJ/mol}))\end{array}}{\text{Dischargepower(kW)}}\right) \times 100\% \quad (9)$$

2.2. Catalyst synthesis and reduction

The γ-Al_2O_3 supported metal catalysts (10 wt.% M/γ-Al_2O_3, M = Cu, Ni, Fe or Ru) were prepared via the wetness impregnation method using the corresponding metal salts ($Cu(NO_3)_2{\cdot}3H_2O$, $Ni(NO_3)_2{\cdot}6H_2O$, $Fe(NO_3)_3{\cdot}9H_2O$, $RuCl_3{\cdot}3H_2O$, respectively). A solution of metal salts (commercially sourced) was first prepared. The alumina beads were then added to the solution and continuously stirred for 16 h. Following this, the water was evaporated off using a water bath at 80 °C. The samples were then dried at 110 °C for 16 h and subsequently calcined at 500 °C for 5 h. The prepared catalysts shall be referred to as 10Cu, 10Ni, 10Fe and 10Ru, where 10 stands for weight % of the metals in the catalysts.

The reduction of the calcined catalysts was performed in a tube furnace using 50 mL/min flow of H_2 for 2 h. The reduction temperatures of 10Cu, 10Ni, 10Fe and 10Ru were 350, 700, 700 and 250 °C, respectively, and were determined using H_2-temperature-programmed reduction (H_2-TPR) (data not presented here). Following the reduction stage, the catalysts were first purged in N_2 for 15 min (50 mL/min) and then underwent passivation in premixed 0.5 vol.%O_2 - 95 vol.% N_2 gas mixture for 6 h (50 mL/min). The catalysts were further reduced in a H_2 plasma (30 mL/min and 16 W discharge power) in the DBD reactor (Fig. 1) for 30 min prior to the plasma-catalytic CO_2 hydrogenation, to remove oxygen from the catalyst surface following the passivation.

2.3. Catalyst characterisation

Powder x-ray diffraction (XRD) was used to identify the phases present in each of the catalysts tested in this work. XRD patterns were recorded in the range $2\theta = 20-90$ ° at a step width of 0.05 ° using a Bruker AXS with a Cu Kα radiation at a wavelength of 0.154 nm. The surface area, pore volume and pore size of each catalyst was determined using a Micromeritics BET Surface Area Analyser. The degassing temperature was 200 °C with a duration of 24 h.

3. Results

3.1. Catalyst characterisation

X-ray diffraction was carried out on the fresh catalysts, after

calcination but prior to reduction. Clear peaks for Al_2O_3 can be seen in all XRD patterns (Fig. 3). Iron oxide was in the form of α-Fe_2O_3, whilst copper and ruthenium were in the oxide forms of CuO and RuO_2, respectively. The XRD peaks for RuO_2 were the narrowest and most intense, whilst no peaks for NiO could be distinguished. The lack of nickel oxide peaks signifies a high dispersion of nickel oxide on the alumina support. The narrow XRD peaks of CuO and RuO_2 reveal a small crystallite size.

XRD was also performed on the catalysts after the reaction had taken place. Both the nickel and copper catalysts were clearly reduced from their oxide forms and were not re-oxidised during the course of the reaction, as Fig. 3 (a) and (c) show the metals are present in their metallic forms (10Ni and 10Cu). Considering the 10Fe and 10Ru catalysts, (Fig. 3 (b) and (d)), it can be seen that after the reaction these metals are present in both their metallic and oxide forms. The 10Ru catalyst mainly consists of metallic Ru, with only two peaks for RuO_2. The spent 10Fe catalyst XRD pattern contains only two iron peaks: one peak for the metallic (Fe) form and one for the oxide (Fe_2O_3) form, the latter of which has a much higher intensity. The 10Fe and 10Ru catalysts are therefore most likely re-oxidised during the reaction, although it cannot be ruled out that the catalysts were not fully reduced in the reduction steps.

The difference in the surface area between the catalysts (Table 1) was only slight and did not follow the trend in conversions achieved in the CO_2 hydrogenation reaction (Fig. 4(a)). Therefore, the surface area, and hence the number of active sites at the catalyst surface, was not the main contributing factor for determining reaction performance. Indeed, all the catalysts had a smaller surface area than the alumina support.

The pore volume was similar for all the catalysts whilst the pore size differed to a greater degree; however, all catalysts had larger pore sizes than the diameter of the CO_2 molecule (0.33 nm) and so diffusion of CO_2 into pores could occur with all catalysts. It is therefore concluded that the difference in pore size should not greatly affect the reaction performance.

Table 1
Surface area, pore volume and pore size of Al_2O_3 and the different metal catalysts tested in the plasma-catalytic methanation reaction, as determined using BET analysis.

Catalyst	BET surface area (m^2/g)	Pore volume (cm^3/g)	Pore size (nm)
Al_2O_3	298	0.42	3.80
10Ni	204	0.39	5.50
10Fe	192	0.44	3.79
10Cu	191	0.40	5.98
10Ru	222	0.45	6.30

3.2. Reaction performance results

3.2.1. Reactant conversions

The presence of alumina beads increased the CO_2 and H_2 conversions from 13.5% and 3.2% to 16.7% and 17.2%, respectively, in comparison to the plasma-only experiment (Fig. 4(a)). 10Fe attained CO_2 and H_2 conversions (8.3% and 10.7%, respectively) below those of Al_2O_3 and a CO_2 conversion lower than the plasma-only experiment (Fig. 4(a)). Interestingly, the conversions of H_2 and CO_2 achieved using 10Cu are above those of Al_2O_3. The addition of 10Ni, 10Cu and 10Ru led to greater improvement of the H_2 conversion than the CO_2 conversion in comparison to the alumina-only experiment.

3.2.2. Product selectivities

In the plasma-only experiment, the major product was CO with a selectivity of over 95% (Fig. 4(b)). The only other product was CH_4. When using a packed bed, the extent to which different reactions occurred was significantly modified. CO_2 conversion increased only slightly but H_2 conversion increased significantly, whilst CO remained the major product. When using Al_2O_3, the selectivity to C_2H_6 increased from 0% (plasma-only) to 16% (Fig. 4(b)). A further increase in hydrocarbon selectivity was seen when the catalysts were combined with plasma. The addition of the catalysts had little effect on the CH_4 selectivity, with only 10Ni improving the CH_4 selectivity in comparison to the

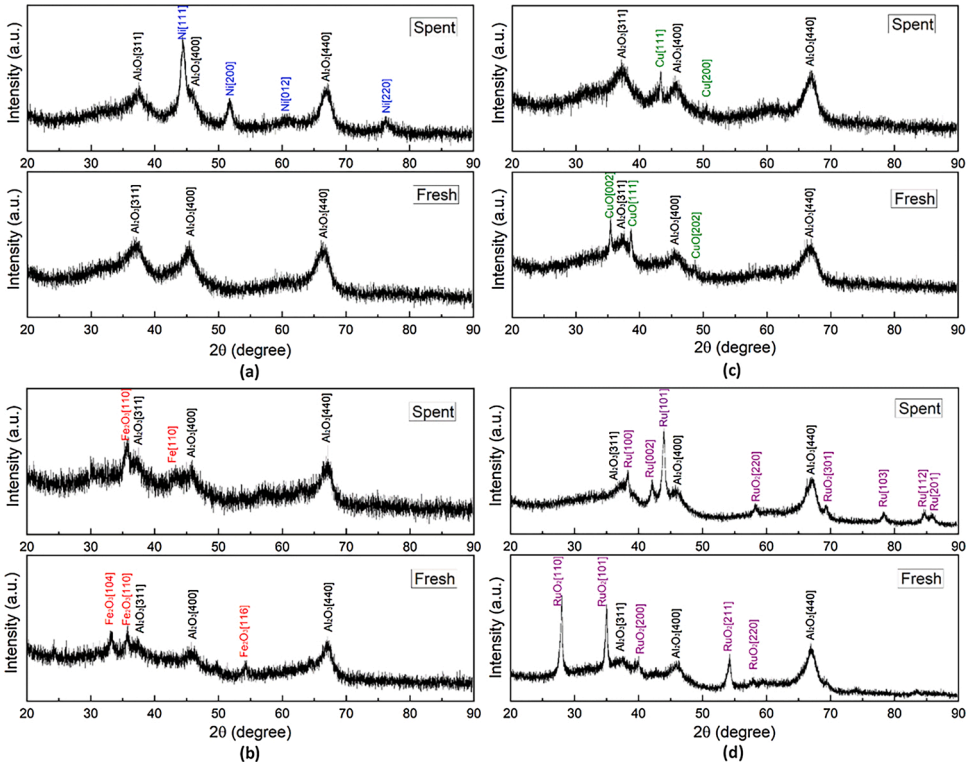

Fig. 3. XRD patterns of fresh (pre-reduction) and spent a) 10Ni; b) 10Fe; c) 10Cu and d) 10Ru catalysts.

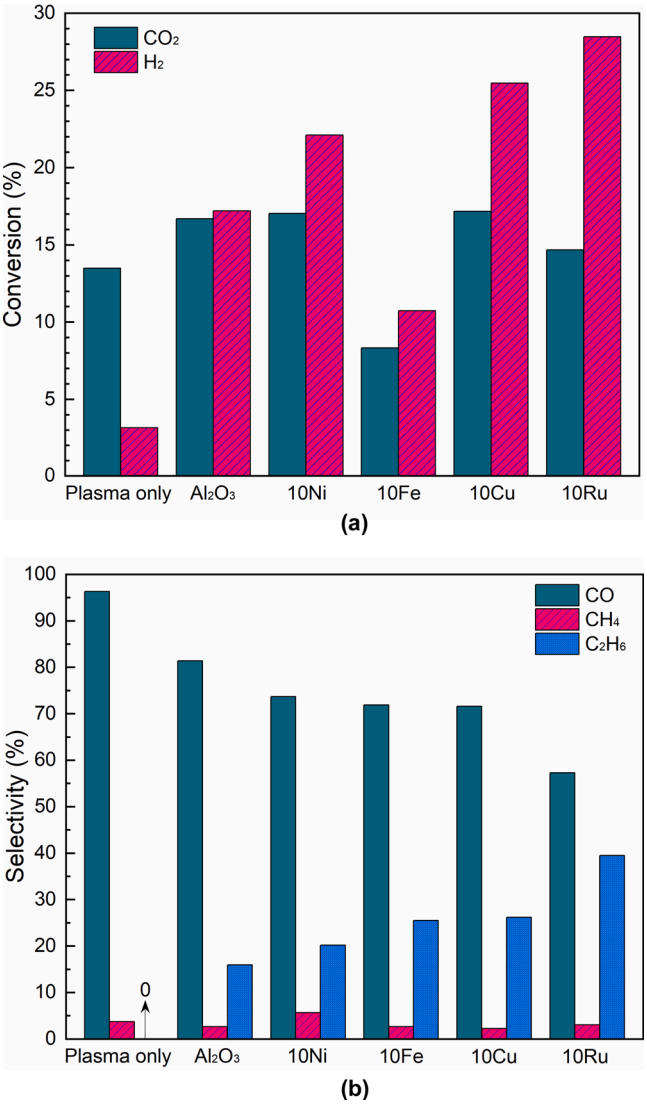

Fig. 4. Reaction performance results of the plasma-only and plasma-catalytic CO_2 hydrogenation experiments a) CO_2 and H_2 conversions; b) Selectivity to main products CO, CH_4 and C_2H_6 (H_2/CO_2 = 4:1, 60 mL/min, 16 W).

plasma-only case, but a significant effect on C_2H_6 selectivity (Fig. 4(b)). The selectivity to C_2H_6 increased in the following order: plasma only (0%) < Al_2O_3 (16%) < 10Ni (20%) < 10Fe (25%) < 10Cu (26%) < 10Ru (39%). On the other hand, the CH_4 selectivity increased according to: 10Cu (2.3%) < Al_2O_3 (2.7%) = 10Fe (2.7%) < 10Ru (3.0%) < plasma only (3.7%) < 10Ni (5.6%). Furthermore, C_2H_4 and C_3H_8 were also found to be possible products of the plasma-catalytic CO_2 methanation reaction (Table 2). Both 10Ni and 10Ru catalysts produced small amounts of C_2H_4, whilst 10Ni also produced C_3H_8. The carbon balance was above 99.8% for all catalysts, implying that all significant products were accounted for.

Table 2
Carbon balance and selectivity to hydrocarbons achieved for the plasma-only and plasma catalytic CO_2 methanation experiments (H_2/CO_2 = 4:1, 60 mL/min, 16 W).

Experiment	Selectivity (%)				Carbon balance (%)
	CH_4	C_2H_4	C_2H_6	C_3H_8	
Plasma only	3.71	0.00	0.00	0.00	99.9
Al_2O_3	2.66	0.00	16.0	0.00	99.8
10Ni	5.64	0.40	20.2	0.09	99.8
10Fe	2.65	0.00	25.5	0.00	99.9
10Cu	2.25	0.00	26.2	0.00	99.8
10Ru	3.03	0.23	39.5	0.00	99.8

3.2.3. *Energy costs and efficiencies*

The addition of Al_2O_3 and all catalysts decreased the energy costs associated with H_2 conversion and CH_4 production in comparison to the plasma-only experiment, whilst the energy cost of CO_2 conversion decreased for all experiments aside from 10Fe (Fig. 5(a and b)). The 10Fe catalyst had the highest energy cost of CO_2 conversion, at 21.3 MJ/mol, due to the low apparent CO_2 conversion, likely resulting from the prevalence of reverse reactions in CO_2 reforming. The H_2 energy cost decreased when using a packed bed. This is because the packed bed increased the electron energies and enhanced the local electric field, resulting in an increase in H_2 conversion without changing the discharge power and H_2 input. The energy cost of CH_4 production was the highest for the plasma-only experiment (13.2 MJ/mol) as the actual number of moles of CH_4 produced was smaller than for the other experiments due to the lower total conversion, even though this experiment resulted in the second highest CH_4 selectivity.

The energy efficiency rose from 3.7% for the plasma-only experiment to a maximum of 17.9% when using 10Ru (Fig. 5(c)). All other catalysts and Al_2O_3 also led to a rise in energy efficiency in comparison to the plasma-only experiment. This was due to the increase in hydrocarbon production attained when using the packed bed reactor.

4. Discussion

Multiple reactions and pathways that convert CO_2 and H_2 into different carbon-containing and non-carbon products can occur. One such reaction is the methanation reaction, known as the Sabatier reaction. The overall reaction is exothermic (Eq. 10); however, it proceeds via a two-step mechanism. Firstly, H_2O and CO are produced from CO_2 and H_2 in the reverse water-gas shift (RWGS) reaction (Eq. 11). Following this, CH_4 is produced via the reaction between H_2 and CO (Eq. 12) [26]. The former reaction is endothermic, whilst the latter is exothermic.

$$CO_2 + 4H_2 \leftrightarrow CH_4 + 2H_2O \Delta H_r = -165\ kJ/mol \quad (10)$$

$$CO_2 + H_2 \leftrightarrow CO + H_2O \Delta H_r = 41\ kJ/mol \quad (11)$$

$$CO + 3H_2 \leftrightarrow CH_4 + 2H_2O \Delta H_r = -206\ kJ/mol \quad (12)$$

Alongside the RWGS reaction, the water-gas shift reaction may also occur, reforming the reactants CO_2 and H_2 (Eq. 13).

$$CO + H_2O \rightarrow CO_2 + H_2 \Delta H_{298} = -41\ kJ/mol \quad (13)$$

Carbon dioxide and hydrogen can also directly react to produce C_2H_6 (Eq. 14).

$$CO_2 + 3.5H_2 \leftrightarrow 0.5C_2H_6 + 2H_2O \Delta H_r = -132\ kJ/mol \quad (14)$$

Carbon is another possible product from the reaction between CO_2 and H_2 (Eq. 15).

$$CO_2 + 2H_2 \leftrightarrow C + 2H_2O\ \Delta H_r = -90\ kJ/mol \quad (15)$$

The formation of carbon via Eq. 15 or through the dissociation of CO (Eq. 16) can lead to the production of CH (Eq. 17) and CH_2 (Eq. 18). CH_2 can also be formed via Eq. 19. Both CH and CH_2 are important intermediates in the production of CH_4. CH is considered the most important intermediate, as the rate coefficient of Eq. 18 is significantly lower than that of Eq. 17 [6].

$$CO + e \rightarrow C + O + e \quad (16)$$

$$C + H_2 \rightarrow CH + H \quad (17)$$

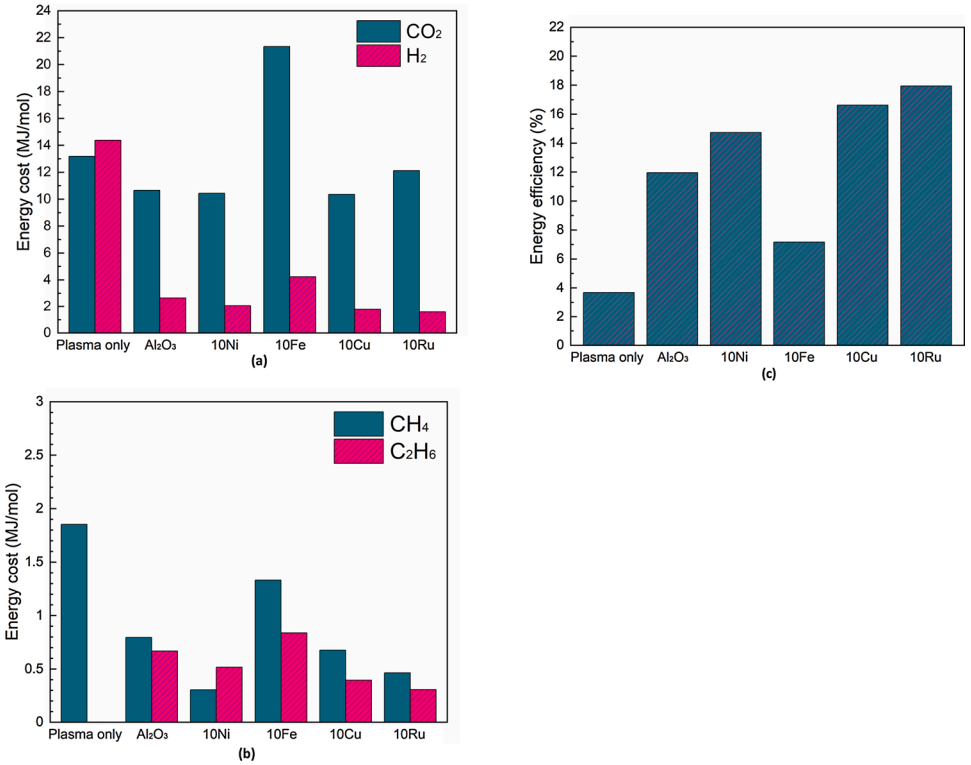

Fig. 5. Reaction performance results of the plasma-only and plasma-catalytic CO_2 hydrogenation experiments: a) Energy cost of CO_2 and H_2 conversion; and b) Energy cost for production of CH_4 and C_2H_6; and c) Energy efficiency (H_2/CO_2 = 4:1, 60 mL/min, 16 W).

$$C + H_2 \rightarrow CH_2 \quad (18)$$

$$H_2 + CH \rightarrow CH_2 + H \quad (19)$$

Following the formation of CH and CH_2 species, CH_4 can form in the plasma phase according to Eq. 20. The produced CH_4 can then dissociate in the plasma to CH_3, CH_2 or CH (Eqs. 21–23) [6]. The CH_x intermediates may also react in the plasma to form higher hydrocarbons, such as C_2H_2 (Eq. 24); whilst C_2H_4 can also be formed via Eqs. 25 and 26.

Several reactions involving CH_x take place in the plasma phase:

$$H_2 + CH_2 \rightarrow CH_4 \quad (20)$$

$$CH_4 + e \rightarrow CH_3 + H + e \quad (21)$$

$$CH_4 + e \rightarrow CH_2 + H_2 + e \quad (22)$$

$$CH_4 + e \rightarrow CH + H + H_2 + e \quad (23)$$

$$CH + CH \rightarrow C_2H_2 \quad (24)$$

$$CH_4 + CH \rightarrow C_2H_4 + H \quad (25)$$

$$CH_2 + CH_3 \rightarrow C_2H_4 + H \quad (26)$$

Reactions that produce CH_x may also take place at the catalyst surface, such as Eqs. 27−29; whilst C_2H_6 can be produced via Eq. 30.

Reactions involving CH_x at the catalyst surface:

$$C_{ads} + H_{ads} \rightarrow CH_{ads} \quad (27)$$

$$CH_{ads} + H_{ads} \rightarrow CH_{2,ads} \quad (28)$$

$$CH_{2,ads} + 2H_{ads} \rightarrow CH_{4,gas} \quad (29)$$

$$CH_3 + CH_3 + M \rightarrow C_2H_6 + M \quad (30)$$

The presence of alumina beads increased the CO_2 and H_2 conversions from 13.5% and 3.2% to 16.7% and 17.2%, respectively, in comparison to the plasma-only experiment (Fig. 4(a)). This can be explained by the packed bed effect on the plasma discharge. When the discharge area is fully packed, breakdown occurs more readily as the electron energy and local electric field increase at the bead contact points where surface discharges can form [7,8,27,28]. In an empty reactor, filamentary discharges are prominent, thus the acceleration of electrons and the electron temperature are reduced in comparison to a packed bed reactor with sufficient void gap volume [7–10,27,28]. The higher mean electron temperature in a packed bed reactor leads to thermodynamic barriers to CO_2 hydrogenation reactions being met, and thus higher conversions of CO_2 and H_2. The reactant conversions are also partially determined by the residence time of the gases in the plasma. It is not possible to know the residence time of the gases in this experiment, as the actual free volume of the reactor cannot be accurately calculated when the reactor is filled with catalyst; hence there is no way of knowing the length of the gas path through the reactor as the gas molecules move through the packed bed. It can be assumed that the residence time of the gases flowing through the empty reactor is below that of the gases flowing through the packed bed reactor; thus, fewer interactions can occur between the reagents and the excited plasma species in the absence of a packed bed. This partially explains the increase in CO_2 and H_2 conversions when using a packed bed in comparison to the empty reactor.

The gases will also interact with the different catalyst surfaces for differing lengths of time, depending on their adsorption/desorption coefficients, which vary between catalyst surfaces. Modelling can be used to gain insights into the plasma-catalyst interactions; however, much of the input data required cannot be found in literature and is outside the scope of this manuscript.

Reaction mechanisms are complex as many reactions take place that convert CO_2 and/or H_2; thus the increase in conversion of each reactant may differ. The product selectivity can aid our understanding of this, as the products indicate the dominant reactions. This is addressed later in the manuscript.

10Fe attained CO_2 and H_2 conversions (8.3% and 10.7%, respectively) below those of Al_2O_3 and a CO_2 conversion lower than the plasma-only experiment (Fig. 4(a)). This catalyst may therefore be catalysing reactions involving the production of CO_2 and H_2 from species created in the plasma. Iron is a well-known water-gas shift reaction catalyst [29,30]; thus 10Fe may have catalysed the production of CO_2 and H_2 from CO and H_2O (Eq. 13). Furthermore, the XRD pattern of spent 10Fe (Fig. 3(b)) showed iron to be present in oxidised form, Fe_2O_3, after the reaction. It is known that Fe_2O_3 can oxidise CO, thus forming CO_2 [31]. This reaction may therefore account for the low CO_2 conversion when using 10Fe, as CO produced in the plasma undergoes oxidation to CO_2 at the catalyst surface. Copper is also a water-gas shift catalyst that typically requires lower temperatures than iron to catalyse the reaction [32–35]. Interestingly, the conversions of H_2 and CO_2 obtained using 10Cu are above those of Al_2O_3; thus, the water-gas shift reaction may occur to a lesser extent when using 10Cu than it does for 10Fe. Copper is also a known catalyst for the production of methanol; however, to produce high yields of methanol, copper usually needs to be combined with zinc oxide, as the activity for methanol production comes from the interaction of Cu and ZnO [36,37]. The interaction between Al_2O_3 and Cu can lead to production of methanol [38], albeit not as successfully as when Cu-ZnO is used. The XRD results revealed copper was present in metallic form after the reaction whilst the Al_2O_3 peaks in 10Cu showed some change in peak intensity and width when comparing the fresh catalyst to the spent catalyst. This may therefore indicate interactions occur between Cu and Al_2O_3 after the catalyst reduction stage. Production of methanol when using alumina for the support depends on the nature of the aluminium active site; this can either favour formation of CO or CH_3OH [38]. As no liquid products were produced or were produced in such small volumes that they couldn't be quantified, and due to the high selectivity towards CO (> 70%), it is theorised that the alumina active site in the Cu catalyst supported the formation of CO over methanol. Similarly to 10Fe, the 10Ru catalyst may have been catalysing the oxidation of CO, as ruthenium was present in both metallic and oxide form in the spent catalyst, as shown by the XRD results. This may explain the low CO_2 conversion over the 10Ru catalyst, which is below that achieved when using alumina-only. The XRD data for 10Ni does not reveal anything in relation to the reactant conversions.

The addition of 10Ni, 10Cu and 10Ru led to greater improvement of the H_2 conversion than the CO_2 conversion in comparison to the alumina-only experiment. As the alumina-only case also led to an increase in H_2 conversion in comparison to the plasma-only experiment, it is concluded that the effect is partially a result of the packed bed which increases the prevalence of gas phase reactions due to the higher electron energy. However, plasma-catalyst interactions or reactions at the catalyst surface must also play a role as the different catalysts increase the H_2 conversion to varying degrees above that obtained when using pure Al_2O_3. Further insights can be gained from studying product selectivities.

According to the Gibbs free energy associated with the most important reaction pathways (Fig. 6 [26]), at temperatures measured in the plasma reactor (< 200 °C), the methanation reaction should be favoured, along with carbon formation and the production of C_2H_6 (since when $\Delta G < 0$, the forward reaction is favoured). However, the water-gas shift (WGS) reaction is also favoured. As methane formation can occur according to the two-step mechanism (Eqs. 11 and 12), whereby CO must first be formed from the RWGS reaction, the production of methane and the WGS reaction must be competing. Furthermore, CO produced from CO_2 dissociation can also contribute in the WGS reaction; hence decreasing the apparent CO_2 and H_2 conversions as well as the CH_4 selectivity. The low H_2 conversion may also be attributed to the recombination of dissociated hydrogen.

Reactions forming C, CH and CH_2, the intermediates to CH_4 and C_2H_6 production, must be catalyst-dependant as the CH_4 selectivity and the C_2H_6 selectivity differ between the catalysts. In plasma, the formation of hydrocarbons can result from a series of radical reactions occurring in the gas phase, following CO_2 and H_2 dissociation. CH_x radicals are first produced before further reactions lead to the formation of C_xH_y [39]. CH_x can also be produced at the catalyst surface; hence the selectivity will be catalyst-dependant.

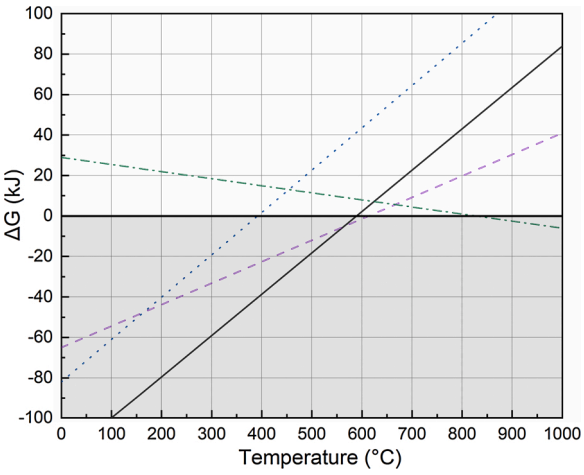

Fig. 6. Gibbs free energy associated with reactions involved in the CO_2 hydrogenation process, as a function of temperature, adapted from [26].

In the plasma-only experiment, the major product was CO with a selectivity of over 95% (Fig. 4(b)). The only other product was CH_4. The reaction between CO_2 and H_2 to form CH_4 (Eq. 10) did not dominate; neither did the reverse water gas shift reaction (Eq. 11), as evidenced by the lack of liquid products, which was limited by the low bulk gas temperature in the plasma [40]. Water may have been present as vapour; however, given that a GC with molecular sieve was used to quantify the products, water was therefore removed by the GC prior to gas detection and thus could not be detected. Selectivity to CH_4, C_2H_6 and other hydrocarbons is limited in the plasma-only case due to the number of reactions required to form these products in the gas phase, combined with a low residence time and no catalytic effect; hence no surface was provided for reactions Eqs. 27–29 to occur on. Excited hydrogen species may instead recombine downstream of the reactor. The product CO was most likely produced directly from CO_2 dissociation, as this accounts for the high selectivity to CO along with the greater CO_2 conversion in comparison to H_2 conversion. However, recombination of CO and O can occur; this reaction, along with the high stability of the CO_2 molecule, explains the obtained overall low CO_2 conversion. The major reaction pathway in the plasma-only experiment was therefore CO_2 dissociation, whilst reactions (Eqs. 10–12 and Eqs. 27–29) occurred to a limited extent. This is unusual in the plasma CO_2 hydrogenation process as the CO_2 methanation and reverse water-gas shift reactions usually dominate due to the lower thermodynamic barrier in comparison to CO_2 dissociation [41].

When using a packed bed, the extent to which different reactions occurred was changed significantly. CO_2 conversion increased only slightly but H_2 conversion increased significantly, whilst CO remained the main product. The reverse water-gas shift reaction (Eq. 11) therefore occurred to a greater extent when fully packing the discharge gap in comparison to the empty reactor. As well as increasing the conversions of H_2 and CO_2, the packed bed effect can also increase the selectivity to higher hydrocarbons. When using Al_2O_3, the selectivity to C_2H_6 increased from 0% (plasma-only) to 16% (Fig. 4(b)) as the rise in local electric field due to the packed bed can result in radical reactions involving CH_x species occurring more readily (Eqs. 21−23) [42]. CH_3 species can then combine according to Eq. 30, with the extent of reaction limited due to the low activity of alumina as a surface for this reaction. A further increase in hydrocarbon selectivity was seen when the catalysts were combined with plasma due to the creation of new reaction pathways at the catalyst surface.

Interestingly, the addition of the catalysts had little effect on the CH_4 selectivity, with only 10Ni improving the CH_4 selectivity in comparison to the plasma-only case, but a significant effect on C_2H_6 selectivity (Fig. 4 (b)). The selectivity to C_2H_6 increased in the order: plasma only (0%) < Al_2O_3 (16%) < 10Ni (20%) < 10Fe (25%) < 10Cu (26%) < 10Ru (39%); whilst the CH_4 selectivity increased according to: 10Cu (2.3%) < Al_2O_3 (2.7%) = 10Fe (2.7%) < 10Ru (3.0%) < plasma only (3.7%) < 10Ni (5.6%). C_2H_4 and C_3H_8 were also found to be possible products of the plasma-catalytic CO_2 methanation reaction (Table 2). Both 10Ni and 10Ru produced small amounts of C_2H_4, whilst 10Ni also produced C_3H_8.

At the catalyst surface, adsorbed C and H species can react to form CH_4 (Eqs. 27–29) [43]; CH_4 created at the catalyst surface desorbs into the gas phase and is therefore available to take part in gas phase reactions to form C_2H_6. Additionally, C_2H_6 can be formed via reaction Eq. 14[26]. This reaction is favoured at temperatures found in the plasma reactor (< 200 °C). C_2H_6 is much more stable than other hydrocarbons [26]; hence accounting for the significantly higher C_2H_6 selectivity in comparison to other C_2 and C_3 hydrocarbons. Another route for the formation of C_2H_6 is via dissociation of CH_4 to CH_3 radicals (Eq. 21). These CH_3 radicals can then combine to form C_2H_6 (Eq. 30). This may explain the low CH_4 selectivity but high selectivity towards C_2H_6, as produced CH_4 is converted to C_2H_6 via the CH_3 radical. C_2H_4 can be produced from CH_4 via Eq. 25, or from the reaction between CH_3 and CH_2 (Eq. 26), which are themselves products of CH_4 dissociation (Eqs. 21 and 22. A greater electron energy is required to dissociate CH_4 to CH_2 than to CH_3. The selectivity to C_2H_4 was therefore much lower than the selectivity to C_2H_6 as CH_3 radicals were formed more easily than CH_2 radicals [44]. CO_2 and H_2 conversions and hydrocarbon selectivities can therefore be enhanced when using a packed bed reactor with an appropriate catalyst due to the creation of new reaction pathways at the catalyst surface that occur alongside gas-phase reactions [43].

It is clear from this that the use of a fully packed bed can be detrimental for the production of CH_4 but still be favourable for the production of C_2H_6, as CH_4 is dissociated to CH_3 radicals due to the higher electron energy resulting from the presence of the packed bed, following which the CH_3 radicals recombine to C_2H_6 due to the formation of new pathways at the catalyst surface. The only catalyst that increased the CH_4 selectivity above that of the plasma-only case was 10Ni; thus, this catalyst was the most suited to the plasma-catalytic CO_2 methanation reaction. To maximise the C_2H_6 yield, 10Ru was the most active catalyst; thus reaction Eq. 30 occurred to the greatest extent in the presence of 10Ru in comparison to the other catalysts tested. The carbon balance was almost 100% for all experiments (Table 2); thus, no other significant carbon-containing products were formed.

As stated above, most published literature focusses on production of CH_4; when considering the production of C_2H_6, CO_2 conversions are lower. Lan et al. [3] achieved a maximum C_2-C_4 selectivity of 13.7% at a CO_2 conversion of 45% when using a Co/ZSM-5 catalyst. The work from Lan et al. also reported on Ni and Cu metals, however the support was ZSM-5; interestingly, no hydrocarbons were produced over the Cu/ZSM-5 catalyst. This differs to the findings of the present study, in which the 10Cu supported on alumina achieved the second highest selectivity towards C_2H_6 (26%). The support, and interactions between the metal catalyst and support, may therefore play a significant role in determining reaction performance, as detailed in Ref. [12] for a series of Ni catalysts supported on various zeolites based on silicate-1. Further study into the catalyst-support interactions for the alumina-supported catalysts presented in the current study would be an interesting future area of research, aiming to understand and optimise the interactions for production of C_2H_6.

The maximum C_2H_6 selectivity achieved in the present work was 39%, at a CO_2 conversion of around 15%. Clearly, for the production of C_2H_6, the process presented here is superior to previous studies which achieved maximum C_{2+} selectivities of 26% [3] and 7% [2], unless external heating was employed in the latter; however, even with external heating, the maximum selectivity towards C_{2+} hydrocarbons was 17% at 62% CO_2 conversion [2]. A recycle stream could be used to overcome the relatively low CO_2 conversion in the present work, with multiple passes ensuring all CO_2 is converted and none is released to the atmosphere. Alternatively, using a higher voltage may also increase the conversion, although this is typically associated with a decrease in energy efficiency as the increase in reagent conversion is not proportional to the increase in the plasma power (see Eq. 9).

5. Conclusion

Ethane is an important chemical with many uses and the plasma-assisted production of C_2H_6 in the presence of a metal (most notably ruthenium) catalyst is demonstrated in this work. The high selectivity towards C_2H_6, especially in comparison to previous works, increases the viability of producing C_2H_6 using plasma-catalysis. The addition of a catalyst into the DBD reactor resulted in a significant increase in H_2 conversion, from 3.2% for the plasma-only case to 28.5% for the 10Ru catalyst; however, the CO_2 conversion only increased by a maximum of 3.7%, when using 10Cu (from 13.5% to 17.2%). The CH_4 selectivity decreased for all catalysts apart from 10Ni, which gave a 1.9% increase. The 10Ru catalyst had the highest selectivity towards C_2H_6, in comparison to the other catalysts, at almost 40%. Further work is required to elucidate reaction mechanisms by, for example, using in-situ FTIR techniques and/or modelling to better understand the formation of surface intermediates and the plasma-assisted surface reactions. Future research into the interactions between catalyst and support, as well as those between the catalyst and plasma, would aid greater insight and allow the catalyst to be optimised for the production of ethane, C_2H_6, at industry-relevant scale.

Data availability

No data was used for the research described in the article.

CRediT authorship contribution statement

Bryony Ashford: Conceptualization, Methodology, Investigation, Validation, Formal analysis, Visualization, Writing - original draft, Writing - review & editing. **Chee-Kok Poh:** Investigation, Writing - review & editing. **Kostya (Ken) Ostrikov:** Writing - review & editing. **Luwei Chen:** Conceptualization, Supervision, Writing - review & editing, Project administration, Funding acquisition. **Xin Tu:** Conceptualization, Supervision, Writing - review & editing, Project administration, Funding acquisition.

Declaration of Competing Interest

The authors declare that they have no known competing financial interests or personal relationships that could have appeared to influence the work reported in this paper.

Acknowledgements

This work was supported by the British Council Newton Fund Researcher Links Programme (Grant No. 2020-RLWK12-10284), Doctoral Training Program at the University of Liverpool (UK) and the A* STAR Research Attachment Program (ARAP). This project has received funding from the European Union's Horizon 2020 research and innovation programme under the Marie Skłodowska-Curie grant agreement No. 823745.

References

[1] B. Wang, M. Mikhail, S. Cavadias, M. Tatoulian, P. Da Costa, S. Ognier, Improvement of the activity of CO_2 methanation in a hybrid plasma-catalytic process in varying catalyst particle size or under pressure, J. CO2 Util. 46 (2021), 101471.

[2] J. Wang, M.S. AlQahtani, X. Wang, S.D. Knecht, S.G. Bilén, C. Song, W. Chu, One-step plasma-enabled catalytic carbon dioxide hydrogenation to higher hydrocarbons: significance of catalyst-bed configuration, Green Chem. 23 (2021) 1642–1647.

[3] L. Lan, A. Wang, Y. Wang, CO_2 hydrogenation to lower hydrocarbons over ZSM-5-supported catalysts in a dielectric-barrier discharge plasma reactor, Catal. Commun. 130 (2019), 105761.

[4] S. Saeidi, S. Najari, V. Hessel, K. Wilson, F.J. Keil, P. Concepción, S.L. Suib, A. E. Rodrigues, Recent advances in CO_2 hydrogenation to value-added products — current challenges and future directions, Prog. Energy Combust. Sci. 85 (2021), 100905.

[5] H. Chen, Y. Mu, Y. Shao, S. Chansai, H. Xiang, Y.L. Jiao, C. Hardacre, X. Fan, Nonthermal plasma (NTP) activated metal–organic frameworks (MOFs) catalyst for catalytic CO_2 hydrogenation, AIChE J. 66 (2020), e16853.

[6] Y. Zeng, X. Tu, Plasma-catalytic hydrogenation of CO_2 for the cogeneration of CO and CH_4 in a dielectric barrier discharge reactor: effect of argon addition, J. Phys. D Appl. Phys. 50 (2017), 184004.

[7] D. Mei, X. Zhu, Y.-L. He, J.D. Yan, X. Tu, Plasma-assisted conversion of CO_2 in a dielectric barrier discharge reactor: understanding the effect of packing materials, Plasma Sources Sci. Technol. 24 (2015), 015011.

[8] K. Van Laer, A. Bogaerts, Improving the conversion and energy efficiency of carbon dioxide splitting in a zirconia-packed dielectric barrier discharge reactor, Energy Technol. 3 (2015) 1038–1044.

[9] X. Duan, Z. Hu, Y. Li, B. Wang, Effect of dielectric packing materials on the decomposition of carbon dioxide using DBD microplasma reactor, AIChE J. 61 (2015) 898–903.

[10] D. Ray, C. Subrahmanyam, CO_2 decomposition in a packed DBD plasma reactor: Influence of packing materials, RSC Adv. 6 (2016) 39492–39499.

[11] M. Ronda-Lloret, Y. Wang, P. Oulego, G. Rothenberg, X. Tu, N.R. Shiju, CO_2 hydrogenation at atmospheric pressure and low temperature using plasma-enhanced catalysis over supported cobalt oxide catalysts, ACS Sustain. Chem. Eng. 8 (2020) 17397–17407.

[12] H. Chen, F. Goodarzi, Y. Mu, S. Chansai, J.J. Mielby, B. Mao, T. Sooknoi, C. Hardacre, S. Kegnæs, X. Fan, Effect of metal dispersion and support structure of Ni/silicalite-1 catalysts on non-thermal plasma (NTP) activated CO_2 hydrogenation, Appl. Catal. B Environ. 272 (2020), 119013.

[13] M. Mikhail, P. Da Costa, J. Amouroux, S. Cavadias, M. Tatoulian, M.E. Gálvez, S. Ognier, Tailoring physicochemical and electrical properties of Ni/$CeZrO_x$ doped catalysts for high efficiency of plasma catalytic CO_2 methanation, Appl. Catal. B Environ. 294 (2021), 120233.

[14] M. Biset-Peiró, R. Mey, J. Guilera, T. Andreu, Adiabatic plasma-catalytic reactor configuration: energy efficiency enhancement by plasma and thermal synergies on CO_2 methanation, Chem. Eng. J. 393 (2020), 124786.

[15] F. Ahmad, E.C. Lovell, H. Masood, P.J. Cullen, K. Ostrikov, J.A. Scott, R. Amal, Low-temperature CO_2 methanation: synergistic effects in plasma-Ni hybrid catalytic system, ACS Sustain. Chem. Eng. 8 (2020) 1888–1898.

[16] B. Wang, M. Mikhail, M.E. Galvez, S. Cavadias, M. Tatoulian, P. Da Costa, S. Ognier, Coupling experiment and simulation analysis to investigate physical parameters of CO_2 methanation in a plasma-catalytic hybrid process, Plasma Process. Polym. 17 (2020), e1900261.

[17] D. Wierzbicki, M.V. Moreno, S. Ognier, M. Motak, T. Grzybek, P. Da Costa, M. E. Gálvez, Ni-Fe layered double hydroxide derived catalysts for non-plasma and DBD plasma-assisted CO_2 methanation, Int. J. Hydrogen Energy 45 (2020) 10423–10432.

[18] R. Benrabbah, C. Cavaniol, H. Liu, S. Ognier, S. Cavadias, M.E. Gálvez, P. Da Costa, Plasma DBD activated ceria-zirconia-promoted Ni-catalysts for plasma catalytic CO_2 hydrogenation at low temperature, Catal. Commun. 89 (2017) 73–76.

[19] M. Nizio, A. Albarazi, S. Cavadias, J. Amouroux, M.E. Galvez, P. Da Costa, Hybrid plasma-catalytic methanation of CO_2 at low temperature over ceria zirconia supported Ni catalysts, Int. J. Hydrogen Energy 41 (2016) 11584–11592.

[20] M. Nizio, R. Benrabbah, M. Krzak, R. Debek, M. Motak, S. Cavadias, M.E. Gálvez, P. Da Costa, Low temperature hybrid plasma-catalytic methanation over Ni-Ce-Zr hydrotalcite-derived catalysts, Catal. Commun. 83 (2016) 14–17.

[21] M.Q. Feliz, I. Polaert, A. Ledoux, C. Fernandez, F. Azzolina-Jury, Influence of ionic conductivity and dielectric constant of the catalyst on DBD plasma-assisted CO_2 hydrogenation into methanol, J. Phys. D Appl. Phys. 54 (2021), 334003.

[22] Y.L. Meng, Y. Liu, Q. Wang, Z.H. Luo, S. Shao, Y.B. Li, Y.X. Pan, Highly dispersed Pt-based catalysts for selective CO_2 hydrogenation to methanol at atmospheric pressure, Chem. Eng. Sci. 200 (2019) 167–175.

[23] L. Wang, Y. Yi, H. Guo, X. Tu, Atmospheric pressure and room temperature synthesis of methanol through plasma-catalytic hydrogenation of CO_2, ACS Catal. 8 (2018) 90–100.

[24] Y. Wang, M. Craven, X. Yu, J. Ding, P. Bryant, J. Huang, X. Tu, Plasma-enhanced catalytic synthesis of Ammonia over a Ni/Al_2O_3 catalyst at Near-Room temperature: insights into the importance of the catalyst surface on the reaction mechanism, ACS Catal. 9 (2019) 10780–10793.

[25] D. Mei, X. Zhu, C. Wu, B. Ashford, P.T. Williams, X. Tu, Plasma-photocatalytic conversion of CO_2 at low temperatures: understanding the synergistic effect of plasma-catalysis, Appl. Catal. B Environ. 182 (2016) 525–532.

[26] T. Schaaf, J. Grünig, M.R. Schuster, T. Rothenfluh, A. Orth, Methanation of CO_2 - storage of renewable energy in a gas distribution system, Energy Sustain. Soc. 4 (2014) 1–14.

[27] D. Ray, P.M.K. Reddy, C. Subrahmanyam, Ni-Mn/Γ-Al_2O_3 assisted plasma dry reforming of methane, Catal. Today 309 (2018) 212–218.

[28] D. Ray, R. Saha, C. Subrahmanyam, DBD plasma assisted CO_2 decomposition: influence of diluent gases, Catalysts 7 (2017) 1–11.

[29] W. Ma, G. Jacobs, U.M. Graham, B.H. Davis, Fischer–tropsch synthesis: effect of K loading on the water–gas shift reaction and liquid hydrocarbon formation rate over precipitated Iron catalysts, Top. Catal. 57 (2014) 561–571.

[30] D. Lee, M.S. Lee, J.Y. Lee, S. Kim, H. Eom, D.J. Moon, K. Lee, The review of Cr-free Fe-based catalysts for high-temperature water-gas shift reactions, Catal. Today 210 (2013) 2–9.

[31] J.-S. Roh, J.-Y. Kim, J.-G. Choi, S.-H. Lee, Kinetics of CO oxidation over unloaded and Pd-loaded alpha-Fe_2O_3 spherical submicron catalysts: photoacoustic investigations at low pressure, Catalysts 8 (2018), 8030098.

[32] C. Lang, X. Se, C. Courson, Copper-based water gas shift catalysts for hydrogen rich syngas production from biomass steam Gasification, Energy Fuels 31 (2017) 12932–12941.

[33] K. Sagata, Y. Kaneda, H. Yamaura, S. Kobayashi, H. Yahiro, Influence of coexisting Al_2O_3 on the activity of copper catalyst for water-gas-shift reaction, Int. J. Hydrogen Energy 39 (2014) 20639–20645.

[34] T. Tabakova, V. Idakiev, G. Avgouropoulos, J. Papavasiliou, M. Manzoli, Highly active copper catalyst for low-temperature water-gas shift reaction prepared via a Cu-Mn spinel oxide precursor, Appl. Catal. A Gen. 451 (2013) 184–191.

[35] R.J. Madon, D. Braden, S. Kandoi, P. Nagel, M. Mavrikakis, J.A. Dumesic, Microkinetic analysis and mechanism of the water gas shift reaction over copper catalysts, J. Catal. 281 (2011) 1–11.

[36] T. Lunkenbein, J. Schumann, M. Behrens, R. Schlögl, M.G. Willinger, Formation of a ZnO overlayer in industrial Cu/ZnO/Al_2O_3 catalysts induced by strong metal-support interactions, Angew. Chem. Int. Ed. 54 (2015) 4544–4548.

[37] C. Tisseraud, et al., The Cu-ZnO synergy in methanol synthesis from CO_2, Part 2: origin of the methanol and CO selectivities explained by experimental studies and a sphere contact quantification model in randomly packed binary mixtures on Cu-ZnO coprecipitate catalysts, J. Catal. 330 (2015) 533–544.

[38] E. Lam, J.J. Corral-Pérez, K. Larmier, G. Noh, P. Wolf, A. Comas-Vives, A. Urakawa, C. Copéret, CO_2 Hydrogenation on Cu/Al_2O_3: Role of the Metal/Support Interface in Driving Activity and Selectivity of a Bifunctional Catalyst, Angew. Chem. Int. Ed. 58 (2019) 13989–13996.

[39] C. De Bie, J. Dijk, A. Van & Bogaerts, CO_{2h}ydrogenation in a dielectric barrier discharge plasma revealed, J. Phys. Chem. C 120 (2016) 25210–25224.

[40] J. Polanski, T. Siudyga, P. Bartczak, M. Kapkowski, Environmental oxide passivated Ni-supported Ru nanoparticles in silica: a new catalyst for low-temperature carbon dioxide methanation, Appl. Catal. B Environ. 206 (2017) 16–23.

[41] Y. Zeng, X. Tu, Plasma-catalytic CO_2 hydrogenation at low temperatures, IEEE Trans. Plasma Sci. 44 (2016) 405–411.

[42] C. Liu, G. Xu, T. Wang, Non-thermal plasma approaches in CO_2 utilization, Fuel Process. Technol. 58 (1999) 119–134.

[43] E. Jwa, S.B. Lee, H.W. Lee, Y.S. Mok, Plasma-assisted catalytic methanation of CO and CO_2 over Ni – zeolite catalysts, Fuel Process. Technol. 108 (2013) 89–93.

[44] H. Puliyalil, D. Lašič Jurković, V.D.B.C. Dasireddy, B. Likozar, A review of plasma-assisted catalytic conversion of gaseous carbon dioxide and methane into value-added platform chemicals and fuels, RSC Adv. 8 (2018) 27481–27508.